Le Vine DM, Zaitzeff JB, D'Sa EJ *et al.* (2000) Sea surface salinity: toward an operational remote-sensing system. In: Halpern D (ed.) *Satellites, Oceanography and Society*, pp. 321–335. Elsevier Science.

Miller JL, Goodberlet MA and Zaitzeff JB (1998) Airborne salinity mapper makes debut in coastal zone. *EOS Transactions of the American Geophysical Union* 79: 173–177.

Sallenger AH Jr, Krabill W, Brock J *et al.* (1999) *EOS Transactions of the American Geophysical Union* 80: 89–93.

Sandidge JC and Holyer RJ (1998) Coastal bathymetry from hyper-spectral observations of water radiance. *Remote Sensing Environment* 65: 341–352.

AIR–SEA GAS EXCHANGE

B. Jähne, University of Heidelberg, Heidelberg, Germany

doi:10.1006/rwos.2001.0060

Introduction

The exchange of inert and sparingly soluble gases including carbon dioxide, methane, and oxygen between the atmosphere and oceans is controlled by a thin 20–200 μm thick boundary layer at the top of the ocean. The hydrodynamics in this layer are significantly different from boundary layers at rigid walls since the orbital motion of the waves is of the same order as the velocities in the viscous boundary layer. Laboratory and field measurements show that wind waves and surfactants significantly influence the gas transfer process. Because of limited experimental techniques, the details of the mechanisms and the structure of the turbulence in the boundary layer at a wavy water surface are still not known. A number of new imaging techniques are described that give direct insight into the transfer processes and promise to trigger substantial theoretical progress in the near future.

Theory

Mass Boundary Layers

The transfer of gases and volatile chemical species between the atmosphere and oceans is driven by a concentration difference and the transport by molecular and turbulent motion. Both types of transport processes can be characterized by diffusion coefficients, denoted by D and K_c, respectively. The resulting flux density j_c is proportional to the diffusion coefficient and the concentration gradient. Thus

$$j_c = (D + K_c(z))\nabla c \qquad [1]$$

where z is the vertical distance from the water surface. In a stationary homogeneous case and without sinks and sources by chemical reactions the flux density j is in vertical direction and constant. Then integration of eqn [1] yields vertical concentration profiles

$$C(z_r) - C(0) = j_c \int_0^{z_r} \frac{1}{D + K_c(z)} \mathrm{d}z \qquad [2]$$

The molecular diffusion coefficient is proportional to the velocity of the molecules and the free length between collisions. The same concept can be applied to turbulent diffusion coefficients. Far away from the interface, the free length (called mixing length) is set proportional to the distance from the interface and the turbulent diffusion coefficient K_c for mass transfer is

$$K_c = \frac{\kappa}{Sc_t} u_\star z \qquad [3]$$

where $\kappa = 0.41$ is the von Kármán constant, $u_\star$, the friction velocity, a measure for the velocity fluctuations in a turbulent flow, and $Sc_t = K_m/K_c$ the turbulent Schmidt number. Closer to the interface, the turbulent diffusion coefficients are decreasing even faster. Once at critical length scale l is reached, the Reynolds number $R_e = u_\star l/\nu$ (ν is the kinematic viscosity, the molecular diffusion coefficient for momentum) becomes small enough so that turbulent motion is attenuated by viscosity. The degree of attenuation depends on the properties of the interface. At a smooth solid wall, $K_c \propto z^3$, at a free water interface it could be in the range between $K_c \propto z^3$ and $K_c \propto z^2$ depending on surface conditions.

In any case, two boundary layers are formed. When the turbulent diffusivity becomes equal to the kinematic viscosity, the edge of the viscous boundary layer is reached. As the name implies, this layer is dominated by viscous dissipation and the velocity profile becomes linear because of a constant diffusivity. The edge of the mass boundary layer is reached when the turbulent diffusivity becomes equal to the molecular diffusivity. The relative thickness of both boundary layers depends on the dimensionless ratio $Sc = \nu/D$ (Schmidt number).

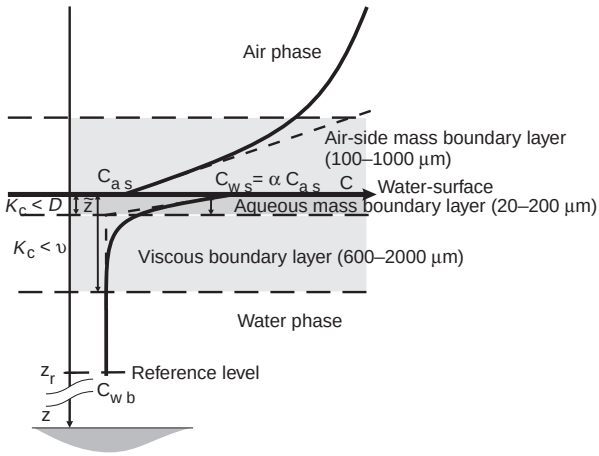

Figure 1 Schematic graph of the mass boundary layers at a gas–liquid interface for a tracer with a solubility $\alpha = 3$.

Boundary layers are formed on both sides of the air-water interface (**Figure 1**). The viscous and mass boundary layers are of about the same thickness in the air, because values of D for various gaseous species and momentum are about the same (Sc_{air} is 0.56 for H_2O, 0.63 for heat, and 0.83 for CO_2). In the liquid phase the situation is completely different. With Schmidt numbers in the range of 100–3000 (**Figure 2**, **Tables 1** and **2**), molecular diffusion for a dissolved volatile chemical species is two to three orders of magnitude slower than diffusion of momentum. Thus the mass boundary layer is significantly thinner than the viscous boundary layer in the liquid phase. This means that the transfer of gases is much slower and almost entirely controlled by the tiny residual turbulence in the small top fraction of the viscous boundary layer. This basic fact makes it difficult to investigate the mechanism of air–water gas transfer both theoretically and experimentally. In addition, the transfer process depends strongly on the water temperature because the Schmidt number decreases by about a factor of 6 from 0 to 35°C (**Table 2**).

Transfer velocity and transfer resistance The amount of species exchanged between the air and water across the interface can be described by a quantity with the units of a velocity. It represents the velocity with which a tracer is pushed by an imaginary piston across the surface. This quantity is known as the transfer velocity k (also known as the piston velocity, gas exchange rate or transfer coefficient). It is defined as the flux density divided by the concentration difference between the surface and the bulk at some reference level z_r:

$$k = \frac{j_c}{C_s - C_b} \qquad [4]$$

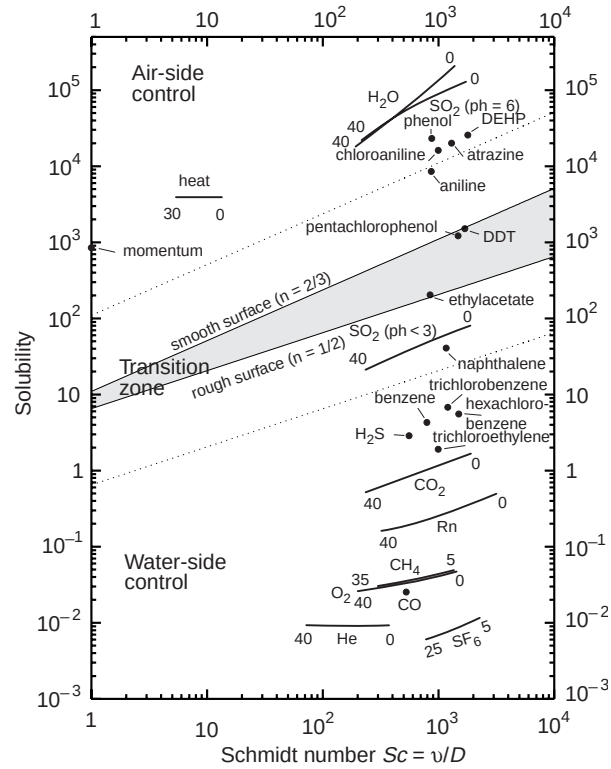

Figure 2 Schmidt number/solubility diagram including various volatile tracers, momentum, and heat for a temperature range (°C) as indicated. Filled circles refer to only a temperature of 20°C. The regions for air-side, mixed, and water-side control of the transfer process between gas and liquid phase are marked. At the solid lines the transfer resistance is equal in both the phases. The following dimensional transfer resistances were used: $r_a = 31$, $r_w = 12Sc^{2/3}$ (smooth), $r_w = 6.5Sc^{1/2}$ (wavy surface) with $r_a = R_a u_{*a}$ and $r_w = R_w u_* w$. Adapted from Jähne and Haußecker (1998).

The inverse of the transfer velocity is known as the transfer resistance R:

$$R = \frac{C_s - C_b}{j_c} \qquad [5]$$

The indices s and b denote the surface and bulk. Both quantities can be directly related to vertical concentration profiles by introducing eqns [4] and [5] into eqn [2]:

$$R = \frac{1}{k} = \int_0^{z_r} \frac{1}{D + K_c(z)}\,\mathrm{d}z \qquad [6]$$

Thus the transfer resistances over several height intervals can be added in the same way as electrical resistances that are connected in series. Typical values of the transfer velocity across the water-side mass boundary layer are 10^{-6}–$10^{-5}\,\mathrm{m\,s^{-1}}$ (1–10 $\mathrm{m\,day^{-1}}$). With respect to typical mixed layer

Table 1 Diffusion coefficients for various gases and volatile chemical species in deionized water and in some cases in sea water. Columns 3 and 4 contain the parameters for the fit of the diffusion coefficient: $D = A \exp[-E_a/(RT)]$, the last four columns the diffusion coefficients for 5, 15, 25, and 35°C

Species	*Molecular mass*	*A* (10^{-5} cm^2 s^{-1})	E_a (kJ mol^{-1})	*σ(Fit) %*	*Diffusion coefficient* (10^{-5} cm^2 s^{-1})			
					5°C	*15°C*	*25°C*	*35°C*
Heat		379.2	2.375		135.80	140.72	145.48	150.08
^{3}He[a,b]	3.02	941	11.70	2.1	5.97	7.12	8.39	9.77
^{4}He	4.00	818	11.70	2.1	5.10	6.30	7.22	8.48
^{4}He[c]		886	12.02	1.8	4.86	5.88	7.02	8.03
Ne	20.18	1608	14.84	3.5	2.61	3.28	4.16	4.82
Kr	83.80	6393	20.20	1.6	1.02	1.41	1.84	2.40
Xe	131.30	9007	21.61	3.5	0.77	1.12	1.47	1.94
^{222}Rn[a]	222.00	15877	23.26	11	0.68	0.96	1.34	1.81
H_2	2.02	3338	16.06	1.6	3.17	4.10	5.13	6.23
H_2[c]		1981	14.93	4.3	3.05	3.97	4.91	5.70
CH_4	16.04	3047	18.36	2.7	1.12	1.48	1.84	2.43
CO_2	44.01	5019	19.51	1.3	1.07	1.45	1.91	2.43
DMS[a]	62.13	2000	18.10		0.80	1.05	1.35	1.71
CH_3Br[a]	94.94	3800	19.10		0.98	1.31	1.71	2.20
F12[a] (CCl_2F_2)	120.91	4100	20.50		0.58	0.79	1.05	1.37
F11[a] (CCl_3F)	137.37	3400	20.00		0.60	0.81	1.07	1.38
SF_6[a]	146.05	2900	19.30		0.69	0.92	1.20	1.55

DMS, dimethylsulfide.
[a]Values of diffusion coefficients from fit, not measured values.
[b]Set 15% higher than ^{4}He.
[c]In sea water.

depths in the ocean of about 100 m, gas transfer is a very slow process. It takes a time constant $\tau = h/k = 10$–100 days for the concentration of dissolved gases in the mixed layer to come into equilibrium with the atmosphere.

Boundary layer thickness The boundary layer thickness $\tilde{z}$ is defined as the thickness of a fictive layer in which the flux is maintained only by molecular transport: $j = D(C_s - C_b)/\tilde{z}$. Then with eqn [4] the boundary layer thickness is

Table 2 Schmidt numbers of various gases and volatile species in the temperature range from 0 to 40°C

Species	*Schmidt number*								
	0°C	*5°C*	*10°C*	*15°C*	*20°C*	*25°C*	*30°C*	*35°C*	*40°C*
Heat	*13.*45	11.19	9.46	8.10	7.02	6.14	5.42	4.82	4.32
^{3}He	329	254	200	160	130	107	88	74	63
^{4}He	379	293	230	184	149	122	102	85	72
^{4}He[a]	402	310	244	194	157	129	107	89	75
Ne	768	579	445	347	276	221	180	148	122
Kr	2045	1478	1090	819	625	483	379	301	241
Xe	2701	1930	1409	1047	791	606	471	370	294
^{222}Rn	3168	2235	1611	1182	883	669	514	400	314
H_2	633	473	360	278	219	174	140	114	94
H_{2a}	648	488	375	293	232	186	151	124	103
CH_4	1908	1400	1047	797	616	483	383	308	250
CO_2	1922	1397	1036	782	600	466	367	293	236
DMS	2593	1905	1428	1089	844	662	527	423	344
CH_3Br	2120	1545	1150	870	669	522	412	329	266
F12 (CCl_2F_2)	3639	2624	1931	1447	1102	851	666	527	422
F11(CCl_3F)	3521	2549	1883	1416	1082	839	658	523	420
SF_6	3033	2208	1640	1239	952	741	585	467	376

[a]In sea water.

given by

$$\tilde{z} = \frac{D}{k} \quad [7]$$

Geometrically, $\tilde{z}$ is given as the intercept of the tangent to the concentration profile at the surface and the bulk (**Figure 1**). Compared to the typical depth of mixed layers or the mean depth of the ocean, the mass boundary layer is extremely thin: 20–200 μm.

Boundary layer time constant The time constant $\tilde{t}$ for the transport across the boundary layer is given by

$$\tilde{t} = \frac{\tilde{z}}{k} = \frac{D}{k^2} \quad [8]$$

Typical values for $\tilde{t}$ are 0.04–4 s. Thus the processes in the mass boundary layer itself are quite fast. Any chemical reaction with a time constant larger than $\tilde{t}$ does not significantly affect the transfer process. Therefore, CO_2 can be regarded as an inert gas but not fastly hydrating acid gases such as SO_2.

The definitions of the three parameters k, $\tilde{z}, \tilde{t}$ are generally valid. They do not depend on any models of the boundary layer turbulence. According to eqns [7] and [8] they are coupled via the molecular diffusion coefficient. Therefore only one of them needs to be measured to obtain knowledge of all three parameters provided the molecular diffusion coefficient of the species is known.

Partitioning of Transfer Between Air and Water

Because a mass boundary layer exists on both sides, it is important to determine which one controls the transfer, i.e., exhibits the largest transfer resistance (or lowest transfer velocity). At the surface itself the thermodynamic solubility equilibrium is assumed to be established between the tracer concentrations c_a in the gas phase and c_w in the liquid phase

$$c_{ws} = \alpha c_{as} \quad [9]$$

where α is the dimensionless solubility (partition coefficient). A solubility $\alpha \neq 1$ causes a concentration jump at the surface (**Figure 1**). Thus the resulting total transfer velocity k_t or transfer resistance R_t can either be viewed from the gas phase or the liquid phase. Adding them up, the factor α must be considered to conserve the continuity of the concentration profile:

$$\text{air side: } \frac{1}{k_{at}} = \frac{1}{k_a} + \frac{1}{\alpha k_w}, \quad R_{at} = R_a + R_w/\alpha$$

$$\text{water side: } \frac{1}{k_{wt}} = \frac{\alpha}{k_a} + \frac{1}{k_w}, \quad R_{wt} = \alpha R_a + R_w \quad [10]$$

The total transfer velocities in air and water differ by the factor α: $k_{at} = \alpha k_{wt}$. The ratio $\alpha k_w/k_a$ determines which boundary layer controls the transfer process. A high solubility shifts control of the transfer process to the gas-phase boundary layer, and a low solubility to the aqueous layer. The solubility value for a transition from air-sided to water-sided control depends on the ratio of the transfer velocities. Typically k_w is about 100–1000 times smaller than k_a. Thus the transfer of even moderately soluble volatile chemical species with solubilities up to 30 is entirely controlled by the water-side. Some environmentally important species lie in a transition zone where it is required to consider both transport processes (**Figure 2**). The transfer of highly soluble volatile and/or chemically reactive gas is controlled by the air-side transfer process and thus analogous to the transfer of water vapor. Therefore, the following considerations concentrate on the water-side transfer process.

Gas Exchange at Smooth Water Surfaces

At smooth water surfaces, the theory of mass transfer is well established because it is equivalent to mass transfer to a smooth solid wall. The turbulent diffusivity can be described by the classic approach of Reichhardt with an initial z^3 increase that smoothly changes to a linear increase in the turbulent layer as in eqn [3]. Then integration of eqn [6] yields the following approximation for Schmidt numbers higher than 60:

$$k_w = u_{\star w} \frac{1}{12.2} Sc^{-2/3} \quad Sc > 60 \quad [11]$$

This equation establishes the basic analogy between momentum transfer and gas exchange. The transfer coefficient is proportional to the friction velocity in water, which describes the shear stress (tangential force per unit area) $\tau = \rho_w u_{\star w}^2$ applied by the wind field at the water surface. Assuming stress continuity at the water surface, the friction velocity in water is related to the friction velocity in air by

$$u_{\star w} = u_{\star a} \left(\frac{\rho_a}{\rho_w} \right)^{1/2} \quad [12]$$

The friction velocity in air, $u_{\star a}$, can further be linked via the drag coefficient to the wind speed U_R at a reference height: $c_D = (u_{\star a} U_R)^2$. Depending on the roughness of the sea surface, the drag coefficient has values between 0.8×10^{-3} and 2.4×10^{-3}. In this way the gas exchange rate is directly linked to the wind speed. The gas exchange further depends on the chemical species and the water temperature via the Schmidt number.

Gas Exchange at Rough and Wavy Water Surfaces

A free water surface is neither solid nor smooth as soon as short wind waves are generated. On a free water surface velocity fluctuations are possible. Thus there can be convergence or divergence zones at the surface; surface element may be dilated or contracted. At a clean water surface dilation or contraction of a surface element does not cause restoring forces, because surface tension only tries to minimize the total free surface area, which is not changed by this process. As a consequence of this hydrodynamic boundary condition, the turbulent diffusivity can now increase with the distance squared from the interface, $K_c \propto z^2$. Then

$$k_w = u_{\star w}\frac{1}{\beta}Sc^{-1/2} \qquad [13]$$

where β is a dimensionless constant.

In comparison to the smooth case in eqn [11], the exponent n of the Schmidt number drops from $-2/3$ to $-1/2$. This increases the transfer velocity for a Schmidt number of 600 by about a factor of 3. The total enhancement depends on the value of the constant β. It is still not well established theoretically for a wavy free water surface.

Influence of Surface Films

A film on the water surface creates pressure that works against the contraction of surface elements. This is the point at which the physicochemical structure of the surface influences the structure of the near-surface turbulence as well as the generation of waves. As at a rigid wall, a strong film pressure at the surface maintains a two-dimensional continuity at the interface. Therefore, eqn [11] should be valid for a smooth film-covered water surface. Eqn [11] has indeed been verified in wind/wave tunnel studies as the lower limit for the transfer velocity. As a consequence, both eqns [11] and eqn [13] can only be regarded as limiting cases. A more general approach is required that has not yet been established. One possibility is a generalization of eqns [11] and [13] to

$$k_w = u_{\star w}\frac{1}{\beta(Sc)}Sc^{-n(Sc)} \qquad [14]$$

where both β and n depend on dimensionless parameters describing the surface conditions (sc). Even films with low film pressure may easily decrease the gas transfer rate to half of its value at clean water surface conditions. However, still too few measurements at sea are available to establish the influence of surfactants on gas transfer for oceanic conditions quantitatively.

Influence of Waves

The waves cannot be regarded as static roughness elements for the liquid flow because their characteristic velocity is of the same order of magnitude as the velocity in the shear layer at the surface. This fact causes a basic asymmetry between the turbulent processes on the air and on the water sides of the interface. Therefore, the wave effect on the turbulent transfer in the water is much stronger and of quite different character than in the air. This basic asymmetry can be seen if the transfer velocity for CO_2 is plotted against the transfer velocity for water vapor (**Figure 3A**). At a smooth water surface the points fall well on the theoretical curve predicted by the theory for a smooth rigid wall. However, as soon as waves occur at the water surface, the transfer velocity of CO_2 increases significantly beyond the predictions.

The surface area increase of a wavy water surface cannot explain this enhancement. Even at high wind speeds, the observed surface increase is well below 20%. When waves are generated by wind, energy is not only transferred via shear stress into the water but a second energy cycle is established. The energy put by the turbulent wind into the wave field is transferred to other wave numbers by nonlinear wave–wave interaction and finally dissipated by wave breaking, viscous dissipation, and turbulent diffusion. The turbulent wave dissipation term is the least-known term and of most importance for enhanced near-surface turbulence. Evidence for enhanced turbulence levels below wind waves has been reported from field and laboratory measurements. Experimental results also suggest that the gas transfer rate is well correlated with the mean square slope of the waves as an integral measure for the nonlinearity of the wind wave field.

Recently, research has focused on microscale wave breaking. A gravity wave becomes unstable, generating a steep train of capillary waves at its leeward face and a turbulent wake. This phenomenon can be observed even at low wind speeds, as soon as wind waves are generated. At higher wind speeds the frequency of microscale wave breaking increases. It is not yet clear, however, to what extent microscale wave breaking can account for the observed enhanced gas transfer rates.

Influence of Breaking Waves and Bubbles

At high wind speeds wave breaking with the entrainment of bubbles may enhance gas transfer further. This phenomenon complicates the gas exchange between atmosphere and the oceans

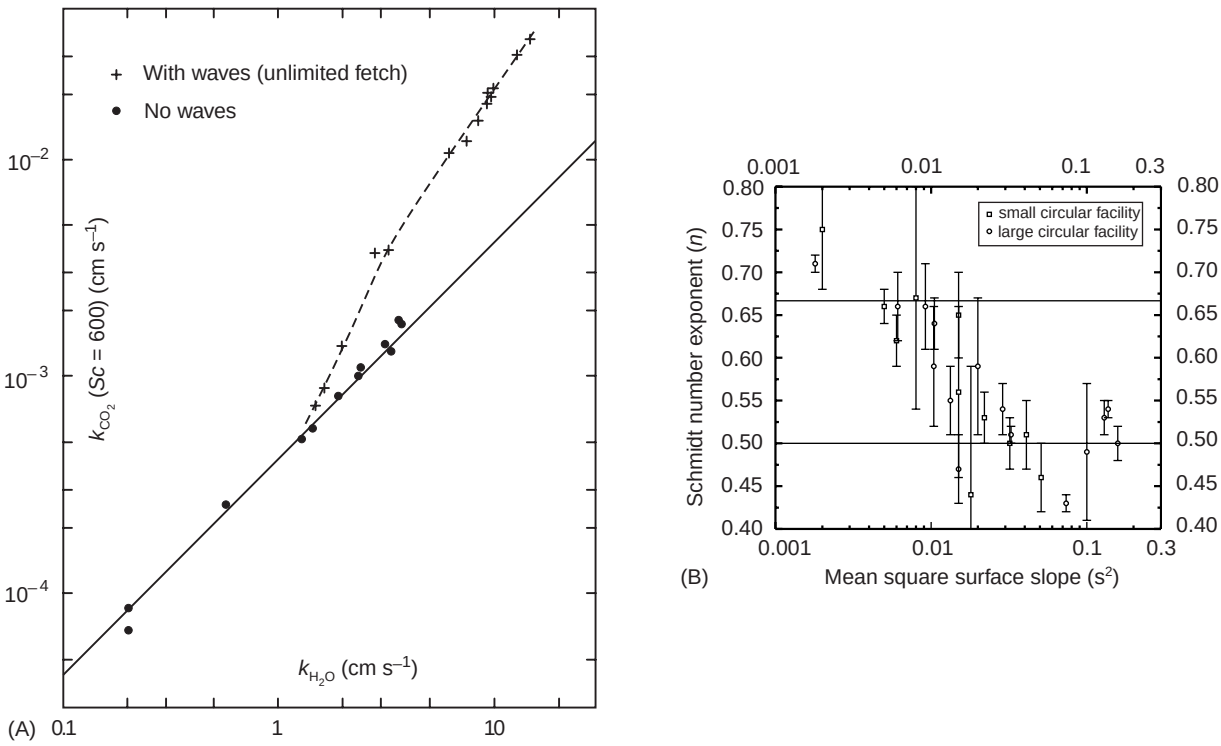

Figure 3 (A) Transfer velocity of CO_2 plotted against the transfer velocity of water vapor as measured in a small circular wind wave facility (Reproduced from Jähne 1980.) (B). Schmidt number exponent n as a function of the mean square slope, (Reproduced from Jähne and Haußecker, 1998.)

considerably. First, bubbles constitute an additional exchange surface. This surface is, however, only effective for gases with low solubility. For gases with high solubility, the gas bubbles quickly come into equilibrium so that a bubble takes place in the exchange only for a fraction of its life time. Thus bubble-mediated gas exchange depends – in contrast to the exchange at the free surface – on the solubility of the gas tracer. Second, bubble-mediated gas transfer shifts the equilibrium value to slight supersaturation due to the enhanced pressure in the bubbles by surface curvature and hydrostatic pressure. Third, breaking waves also enhance near-surface turbulence during the breaking event and the resurfacing of submerged bubbles.

The uncertainties of bubble-mediated gas exchange are even larger than those of the poorly understood influence of nonbreaking waves on air–sea gas transfer. Some experiments from wind/wave tunnels and the field suggest that significant enhancements can occur, other experiments could not observe a significant influence of bubbles. Experimental data are still too sparse for the size and depth distribution of bubbles and the flux of the bubbles through the interface under various sea states for a sufficiently accurate modeling of bubble-mediated air–sea gas transfer and thus a reliable estimate of the contribution of bubbles to the total gas transfer rate.

Empiric Parameterization

Given the lack of knowledge, all theories about the enhancement of gas transfer by waves are rather speculative and are not yet useful for practical application. Thus it is still state of the art to use semiempiric or empiric parameterizations of the gas exchange rate with the wind speed. Most widely used is the parameterization of Liss and Merlivat which identifies three physically well-defined regimes (smooth, wave-influenced, bubble-influenced) and proposes a piece-wise linear relation between the wind speed U and the transfer velocity k:

$$k = 10^{-6} \begin{cases} 0.472U(Sc/600)^{-2/3} & U \le 3.6\,\mathrm{m\,s^{-1}} \\ 7.917(U-3.39)(Sc/600)^{-1/2} & U \le 3.6\,\mathrm{m\,s^{-1}} \\ & \text{and } U \le 13\,\mathrm{m\,s^{-1}} \\ 16.39(U-8.36)(Sc/600)^{-1/2} & U > 13\,\mathrm{m\,s^{-1}} \end{cases} \quad [15]$$

At the transition between the smooth and wavy regime, a sudden artificial jump in the Schmidt num-

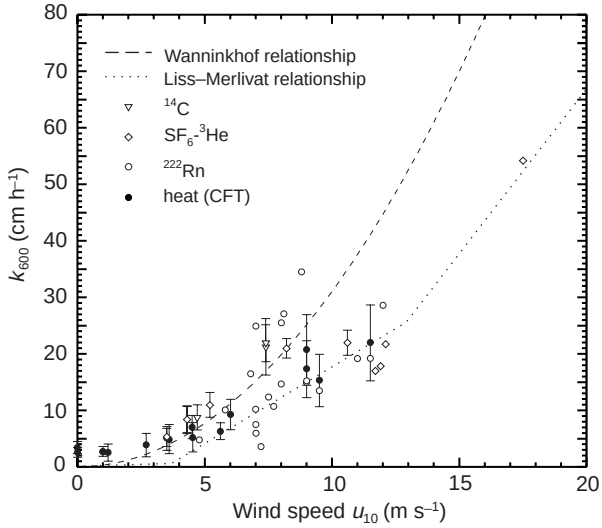

Figure 4 Summary of gas exchange field data normalized to a Schmidt number of 600 and ploted vs. wind speed together with the empirical relationships of Liss and Merlivat (1986) and Wanninkhof (1992). After Jähne and Haußecker (1998).

ber exponent n from 2/3 to 1/2 occurs. This actually causes a discontinuity in the transfer rate for Schmidt number unequal to 600.

Another empiric parameterization simply assumes a quadratic increase of the gas transfer rate with the wind speed:

$$k = 0.861 \times 10^{-6}(\text{s/m})\, U^2 (Sc/600)^{-1/2} \qquad [16]$$

Thus this model has a constant Schmidt number exponent $n = 1/2$. The two parameterizations differ significantly (see **Figure 4**). The second parameterization predicts significantly higher values. The discrepancy between the two parameterizations (up to a factor of two) mirrors the current uncertainty in estimating the air–sea gas transfer rate.

Experimental Techniques and Results

Laboratory Facilities

Laboratory facilities play an important role in the investigation of air–sea gas transfer. Only laboratory studies allow a systematic study of the mechanisms and are thus an indispensible complement to field experiments. Almost all basic knowledge about gas transfer has been gained by laboratory experiments in the past. Among other things this includes the discovery of the influence of waves on air–water gas exchange (**Figure 3A**) and the change in the Schmidt number exponent (**Figure 3B**). Many excellent facilities are available worldwide (**Table 3**). Some of the early facilities are no longer operational or were demolished. However, some new facilities have also been built recently which offer new experimental opportunities for air–water gas transfer studies.

Geochemical Tracer Techniques

The first oceanic gas exchange measurements were performed using geochemical tracer methods such as the ^{14}C, $^3He/T$, or $^{222}Rn/^{226}Ra$ methods. These techniques are based on the mass balance of geochemical tracer in the water body. The volume and time-average flux density is given by mass balance of the tracer concentration in a volume of water V_w

$$V_w \dot{c}_w = F_w j \text{ or } j = h_w \dot{c}_w \qquad [17]$$

where F_w, and h_w are the surface area and the effective height V_w/F_w of a well-mixed water body, respectively. The time constant $\tau_w = h_w/k$ is in the order of days to weeks. It is evident that the transfer velocities obtained in this way provide only values integrated over a large horizontal length scales and timescales in the order of τ_w. Thus a parameterization of the transfer velocity is only possible under steady-state conditions over extended periods. Moreover, the mass balance contains many other sources and sinks besides air–sea gas exchange and thus may cause severe systematic errors in the estimation of the transfer velocity. Consequently, mass balance methods are only poorly suited for the study of the mechanisms of air–water gas transfer.

Tracer Injection

The pioneering lake studies for tracer injection used sulfur hexafluoride (SF_6), a tracer that can easily be measured down to parts per thousand levels with electron-capture detector (ECD) gas chromatography. However, the tracer concentration decreases not only by gas exchange across the interface but also by dispersion of the tracer. This problem can be overcome by the dual tracer technique in which two tracers with different diffusivities (e.g., SF_6 and ^3He) are released. When the ratio of the gas transfer velocities of the two tracers is known, the dilution effect by tracer dispersion can be corrected, making it possible to derive gas transfer velocities. But the basic problem of mass balance techniques, i.e., their low temporal resolution, also remains with artificial tracer approaches.

Eddy Correlation Flux Measurements

Eddy correlation techniques are used on a routine basis in micrometorology, i.e., for tracers controlled by the boundary layer in air (momentum, heat and water vapor fluxes). Direct measurements of the

Table 3 Comparison of the features of some major facilities for small-scale air–sea interaction studies (operational facilities are typeset in boldface)

	KA	*HH*	*M*	*D*	*SIO*	*C*	*UM*	*W*	*SU*	*HD1*	*HD2*	*WH*	*HD3*
Length (mean perimeter) (m)	15	**24**	**40**	100	**40**	**33**	**15**	**18.3**	119	1.57	11.6	**3.14**	**29.2**
Width of water channel (m)	1.8	**1.0**	**2.6**	8.0	**2.4**	**0.76**	**1.0**	**0.91**	2.0	0.10	0.20	**0.20**	**0.62**
Outer diameter (m)	—	—	—	—	—	—	—	—	40	0.60	4.0	**1.2**	**9.92**
Inner diameter (m)	—	—	—	—	—	—	—	—	36	0.40	3.4	**0.8**	**8.68**
Total height (m)	1.5	1.5	**2.0**	3.0	**2.4**	**0.85**	**1.0**	**1.22**	5.6	0.50	0.70	**0.50**	**2.40**
Max. water depth (m)	0.3	**0.5**	**0.8**	0.8	**1.5**	**0.25**	**0.5**	**0.76**	3.0	0.08	0.25	**0.20**	**1.20**
Water surface area (m^2)	27	**24**	**104**	800	**96**	**24.8**	**15**	**16.7**	239	0.16	3.5	**0.63**	**18.0**
Water volume (m^3)	8	**12**	**83**	768	**144**	**8**	10	?	7.16	0.01	0.87	0.13	**20.7**
Maximum wind speed ($m\,s^{-1}$)	15	**25**	**15**	15	**12**	**25**	**30**	**25**	19	11	12	**12**	**12**
Suitable for sea water	N	**N**	**N**	N	**Y**	**N**	**Y**	**N**	Y	Y	Y	**Y**	**Y**
Wave maker	N	**Y**	**Y**	Y	**Y**	**Y**	**Y**	**Y**	N	N	N	**N**	**N**
Water current generator ($m\,s^{-1}$)	Y	**N**	**Y**	Y	**N**	± 0.6	± 0.5	± 0.5	N	N	N	**N**	$< -$**0.6**
Water temperature control (°C)	N	**N**	**Y**	N	**N**	**Y**	**Y**	**Y**	N	5–35	N	**N**	**5–35**
Air temperature control (°C)	N	**N**	**Y**	N	**N**	**N**	**N**	**Y**	N	5–35	N	**N**	**5–35**
Air humidity control	N	**N**	**Y**	N	**N**	**N**	**N**	**N**	N	Y	N	**Y**	**Y**
Gastight air space	N	**N**	**N**	N	**N**	**Y**	**Y**	**Y**	N	Y	Y	**Y**	**Y**

KA, Institute for Hydrology, University of Karlsruhe; HH, Bundesanstalt für Wasserbau, Hamburg; M, IMST, University Marseille, France; D, Delft Hydraulics, Delf, The Netherlands; SIO Hydraulic Facility, Scripps Institution of Oceanography, La Jolla, USA; C, Canada Center for Inland Waters (CCIW); UM, University of Miami; W, NASA Air–Sea Interaction Research Facility, Wallops; SU, Storm basin, Marine Hydrophysical Institute, Sevastopol, Ukraine; HD1, Small annular wind/wave flume, University of Heidelberg; HD2, Large annular wind/wave flume, University of Heidelberg (dismantled); WH, Small annular wind/wave flume Woods Hole Oceanographic Institution (now in Heidelberg); HD3 Aeolotron, University of Heidelberg (HD3, in operation since June 2000).
N = No; Y = Yes.

air–sea fluxes of gas tracers are very attractive because the flux densities are measured directly and have a much better temporal resolution than the mass balance based techniques. Unfortunately, large experimental difficulties arise when this technique is applied to gas tracers controlled by the aqueous boundary layer. The concentration difference in the air is only a small fraction of the concentration difference across the aqueous mass boundary layer. Even after 20 years of research, this technique is not yet well established. Some successful measurements under favorable conditions have been reported but many of the difficulties and complexities associated with the technique are still not resolved.

The Controlled Flux Technique

The basic idea of this technique is to determine the concentration difference across the mass boundary layer when the flux density j of the tracer across the interface is known. The local transfer velocity can be determined by simply measuring the

concentration difference Δc across the aqueous boundary layer according to eqn [4] with a time constant $\tilde{t}$ for the transport across the boundary layer (eqn [8]). This technique is known as the controlled flux technique (CFT).

Heat proves to be an ideal tracer for the CFT. The temperature at the water surface can then be measured with high spatial and temporal resolution using IR thermography. A known and controllable flux density can be applied by using infrared radiation. Infrared radiation is absorbed in the first few micrometers at the water surface. Thus a heat source is put right at the top of the aqueous viscous boundary layer. Then the CFT directly measures the water-side heat transfer velocity.

A disadvantage of the CFT is that the transfer velocity of gases must be extrapolated from the transfer velocity of heat. The large difference in the Schmidt number (7 for heat, 600 for CO_2) casts some doubt on whether the extrapolation to so much higher Schmidt numbers is valid. Laboratory experiments in wind/wave flumes showed, however, that the extrapolation is correct to within error margins of about 10%.

Two techniques proved to be successful. Active thermography uses a CO_2 laser to heat a small spot on the water surface. The heat transfer rates are estimated from the temporal decay of the heated spot. Passive thermography uses the naturally occurring heat fluxes caused by latent heat flux j_l, sensible heat flux j_s and longwave emission of radiation j_r. The net heat flux $j_n = j_l + j_s + j_r$ results according to eqn [4] in a temperature difference across the interface of $\Delta T = j_h/(\rho c_p k_h)$. Because of the turbulent nature of the exchange process any mean temperature difference is associated with surface temperature fluctuations which can be observed in thermal images. With this technique the horizontal structure of the boundary layer turbulence can be observed. Surface renewal is directly observable in the IR image sequences, which show patches of fluid being drawn away from the surface.

With some knowledge about the statistics of the temperature fluctuations, the temperature difference ΔT across the interface as well as the time constant $\tilde{t}$ of heat transfer can be computed from the temperature distribution at the surface. Results obtained with this technique are shown in **Figure 5** and also in the overview graph, **Figure 4**.

Summary of Field Data

A collection of field data is shown in **Figure 4**. Although the data show a clear increase of the transfer velocity with wind speed, there is substantial scatter in the data that can only partly be attributed to uncertainties and systematic errors in the measurements. Thus, in addition, the field measurements reflect the fact that the gas transfer velocity is not simply a function of the wind speed but depends significantly on other parameters influencing near-surface turbulence, such as the wind-wave field and the viscoelastic properties of the surface film.

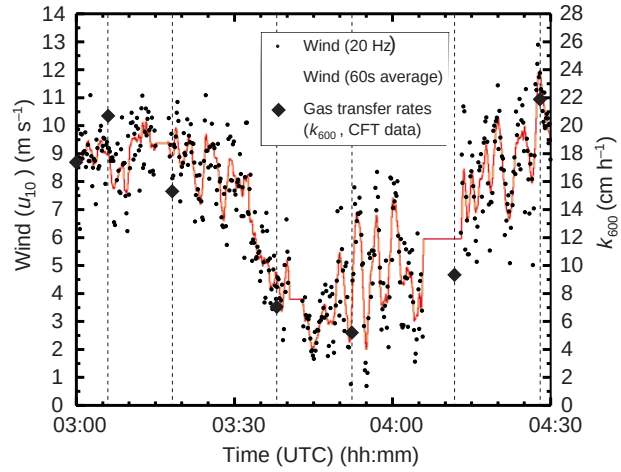

Figure 5 Wind speeds and gas transfer velocities computed with the Controlled Flux Technique (CFT) during the 1995 MBL/CoOP West Coast experiment (JD133) for a period of 90 min. The transfer velocities are normalized to Schmidt number 600 and averaged over 4 minutes each. (Reproduced from Jähne and Haußecker, 1998.)

Outlook

In the past progress towards a better understanding of the mechanisms of air–water gas exchange was hindered by inadequate measuring technology. However, new techniques have become available and will continue to become available that will give a direct insight into the mechanisms under both laboratory and field conditions. This progress will be achieved by interdisciplinary research integrating such different research areas as oceanography, micrometeorology, hydrodynamics, physical chemistry, applied optics, and image processing.

Optical and image processing techniques will play a key role because only imaging techniques give direct insight into the processes in the viscous, heat, and mass boundary layers on both the sides of the air–water interface. Eventually all key parameters including flow fields, concentration fields, and waves will be captured by imaging techniques with sufficient spatial and temporal resolution. The experimental data gained with such techniques will stimulate new theoretical and modeling approaches.

See also

Air–Sea Transfer: Dimethyl Sulphide, COS, CS_2, NH_4, Non-methane Hydrocarbons, Organo-halogens; N_2O, NO, CH_4, CO. Atmospheric Input of Pollutants. Breaking Waves and Near-surface Turbulence. Bubbles. Surface Films. Surface, Gravity and Capillary Waves.

Further Reading

Brutsaert W and Jirka GH (eds) (1984) *Gas Transfer at Water Surfaces*. Hingham, MA: Reidel.

Businger JA and Kraus EB (1994). *Atmosphere–Ocean Interaction*, New York: Oxford University Press.

Donelan M, Drennan WM, Saltzman ES and Wanninkhof R (eds) (2001) *Gas Transfer at Water Surfaces*. Washington DC: American Geophysical Union.

Duce RA and Liss PS (eds) (1997) *The Sea Surface and Global Change*. Cambridge: Cambridge University Press.

Jähne B (1980) *Zur Parameterisierung des Gasaustausches mit Hilfe von Laborexperimenten*, Dissertation, University of Heidelberg.

Jähne B, Haußecker H (1998) Air–water gas exchange. *Annual Review of Fluid Mechanics* 30: 443–468.

Jähne B, Heinz G, and Dietrich W (1987) Measurement of the diffusion coefficients of sparingly soluble gases in water. *Journal of Geophysical Research* 92: 10767–10776.

Jähne B and Monahan E (eds) (1995). *Air–Water Gas Transfer*. Hanau, Germany: Aeon.

King DB, De Bryun WJ, Zheng M and Saltzman ES (1995) Uncertainties in the molecular diffusion coefficient of gases in water for use in the estimation of air–sea exchange. In: Jähne B and Monahan E (eds) *Air–Water Gas Transfer*, pp. 13–22. Hanau, Germany: Aeon.

Liss PS and Merlivat L (1986) Air–sea gas exchange rates: introduction and synthesis. In: Buat-Menard P (ed.) *The Role of Air–Sea Exchange in Geochemical Cycles*, pp. 113–127. Dordrecht, The Netherlands: Reidel.

Wanninkhof R (1992) Relationship between wind speed and gas exchange over the ocean. *Journal of Geophysical Research* 97: 7373–7382.

Wilhelms SC and Gulliver JS (eds) (1991) *Air–Water Mass Transfer*. New York: ASCE.

AIR–SEA TRANSFER

Dimethyl Sulphide, COS, CS_2, NH_4, Non-methane Hydrocarbons, Organo-halogens

J. W. Dacey, Woods Hole Oceanographic Institution, Woods Hole, MA, USA

H. J. Zemmelink, University of Groningen, Haren, The Netherlands

doi:10.1006/rwos.2001.0063

The oceans, which cover 70% of Earth's surface to an average depth of 4000 m, have an immense impact on the atmosphere's dynamics. Exchanges of heat and momentum, water and gases across the sea surface play major roles in global climate and biogeochemical cycling. The ocean can be thought of as a vast biological soup with myriad processes influencing the concentrations of gases dissolved in the surface waters. The quantities of mass flux across the surface interface, though perhaps small on a unit area basis, can be very important because of the extent of the ocean surface and the properties of the gases or their decomposition products in the atmosphere.

Gas exchange across the sea–air surface depends, in part, on differences in partial pressures of the gases between the ocean surface and the atmosphere. The partial pressure of a gas in the gas phase can be understood in terms of its contribution to the pressure in the gas mixture. So the partial pressure of O_2, for example, at 0.21 atm means that at 1 atmosphere total pressure, O_2 is present as 21% of the gas, or mixing, volume. Trace gases are present in the atmosphere at much lower levels, usually expressed as parts per million (10^{-6} atm), parts per billion (10^{-9} atm) or parts per trillion (10^{-12} atm, pptv). Dimethylsulfide (DMS), when present at 100 pptv, accounts for about 100 molecules per 10^{12} molecules of mixed gas phase, or about 10^{-10} of the gas volume.

In solution, a dissolved trace gas in equilibrium with the atmosphere would have the same partial pressure as the gas in the air. Its absolute concentration in terms of molecules or mass per unit volume of water depends on its solubility. Gas solubility varies over many orders of magnitude depending on the affinity of water for the gas molecules and the volatility of the gas. Gases range widely in their solubility in sea water, from the permanent gases like nitrogen (N_2), oxygen (O_2), nitrous oxide (N_2O) and methane (CH_4) that have a low